Hindawi
International Journal of Antennas and Propagation
Volume 2023, Article ID 6553980, 15 pages
https://doi.org/10.1155/2023/6553980

Research Article

Design of a Flexible Cylindrical Antenna with Rotatable Curved Frequency Selective Surface for Omnidirectional High-Gain Applications

Hua Jing,[1,2,3] Ge He,[1] and Shengyao Wang[1]

[1]*School of Aeronautics and Astronautics, University of Electronic Science and Technology of China, Chengdu 611731, China*
[2]*Institute of Electronic and Information Engineering of UESTC in Guangdong, Dongguan 523808, China*
[3]*Aircraft Swarm Intelligent Sensing and Cooperative Control Key Laboratory of Sichuan Province, Chengdu 611731, China*

Correspondence should be addressed to Ge He; hege1009@163.com

Received 5 January 2023; Revised 20 April 2023; Accepted 4 May 2023; Published 15 May 2023

Academic Editor: Flaminio Ferrara

In this paper, a high-gain flexible cylindrical antenna with rotatable curved frequency selective surface (FSS) is presented, which is designed for the 2.4 GHz industrial scientific medical (ISM) band. The array of 3×3 optimized FSS unit cells ($102 \times 102\ mm^2$) is applied to improve the gain of the antenna ($50.4 \times 28 \times 0.1\ mm^3$). Through the rotation of the FSS, omnidirectional gain enhancement is realized. The simulation and measurement results demonstrate the feasibility of this work. The measured antenna with the FSS has omnidirectional high-gain in the operational band of 2.18–2.90 GHz, and the gain can be increased by 5.31 dBi at most. The antenna can be used in cylindrical conformal devices, and the proposed design method provides a new solution for gain enhancement of cylindrical omnidirectional antennas.

1. Introduction

With the rapid development of flexible electronic devices, the research process of flexible antenna is accelerated. The flexible antenna can better adhere to the surface of the carrier, which is more convenient for various special-shaped electronic devices. For example, when an antenna is designed for the compact self-powered devices, the flexible antenna can be bent into a cylindrical shape to fit the dry battery or button battery surface perfectly, which can improve space utilization ratio of the devices.

The microstrip antenna is widely used in the design of a flexible antenna due to its advantages such as light weight, small size and low cost. The realization of flexible antenna depends on the flexible dielectric substrate [1–6]. Common flexible dielectric substrates include polyimide (PI), polydimethylsiloxane (PDMS), and other chemical polymers. In 2022, Liu et al. [7] presented a PI-based flexible monopole antenna, which exhibited excellent deformation capability. Sayem et al. [8] chose the transparent conductive fabric-PDMS composite to fabricate a flexible antenna.

Antenna gain is very important to the operational quality of the wireless communication system. To enhance the gain of antennas, artificial electromagnetic structures such as artificial magnetic conductor (AMC) [9, 10] and frequency selective surface (FSS) [11–15] are proposed as reflectors of antennas. FSS as a spatial filter [16] exhibits different scattering characteristics for electromagnetic waves with different frequencies. Band-stop FSS has total reflection characteristics at resonant frequency, and it is widely used in reflectarray. Retnam et al. [13] used FSS as a back reflector to improve the antenna gain, and an improvement of 3 dBi gain over the operational frequency range of 3.07–3.74 GHz was observed. Devarapalli et al. [14] presented a coplanar waveguide fed elliptical-based second iterative antenna. The peak gain of the antenna was enhanced to 9.48 dBi in *X*-band by loading a single-layer FSS. Moreover, several reflectors designed on the flexible dielectric substrate [17, 18] can be used in various conformal applications.

In this paper, a flexible cylindrical antenna with rotatable curved FSS is proposed. Due to the use of the rotatable curved FSS, the antenna has omnidirectional high-gain characteristics. This method can be applied in the design of high-gain antenna for cylindrical compact electronic devices.

2. Antenna Design

The antenna is intended to be applied in the 2.4 GHz industrial scientific medical (ISM) band (2.400–2.4835 GHz). The proposed coplanar waveguide (CPW)-fed monopole microstrip antenna is shown in Figure 1, and the parameters are shown in Table 1. The size of the antenna is 50.4 mm × 28 mm × 0.1 mm. PI is chosen as the dielectric substrate because it shows good flexibility with dielectric constant 3.5 and loss tangent 0.004. The antenna's radiation pattern in the H plane is omnidirectional.

The design evolution of the antenna is illustrated in Figure 2, and the corresponding simulated reflection return loss (S_{11}) is shown in Figure 3. Firstly, as shown in Figure 2(a), the initial antenna starts with a compact (CPW)-fed antenna, which is named Antenna I. The resonant frequency of a monopole printed antenna can be approximated by the formula (1) given in [19].

$$f_r = \frac{144}{L_g + L_r + g + \left(A_g/2\pi L_g\sqrt{\varepsilon_e}\right) + \left(A_r/2\pi L_r\sqrt{\varepsilon_e}\right)}, \quad (1)$$

where L_g and L_r are the lengths of the ground plane and radiator, g is the gap between them, A_g and A_r are the areas of the ground plane and radiator, and ε_e is the effective dielectric constant.

Next, in Figure 2(b), two corners of the ground are cut off to reduce the coupling effect between the ground and the bottom of the rectangular patch. Finally, in Figure 2(c), a trapezoidal structure is added between the rectangular patch and the feeder line to make impedance matching better. During the optimization process, the parameter scanning method was used to search for the optimal parameter values. Simulation results show that the bandwidth of $S_{11} < -10$ dB is effectively expanded by the above optimization methods. The impedance bandwidth of Antenna III is 1.96–3.61 GHz and the percentage bandwidth is 59.25%.

The proposed antenna is intended to be used in cylindrical conformal devices, and the corresponding simulated conformal model is depicted in Figure 4. The simulation results at different bending radius (R) are shown in Figure 5. When R is 8 mm, the resonant frequency is 2.50 GHz, the bandwidth is 1.94–3.64 GHz, and the percentage bandwidth is 60.93%. For different bending radius, the resonant frequency of the bending antenna is slightly shifted and the impedance bandwidth is decreased. The lowest operational frequency remains stable, but the highest operational frequency is affected by the bending radius. The impedance model of the antenna can be considered as a simple RLC parallel equivalent circuit as illustrated in Figure 6. The different bending radius basically do not change the equivalent circuit structure of the antenna but change the value of equivalent capacitance and inductance. Naturally, the resonant frequency is slightly different but the trend remains basically constant.

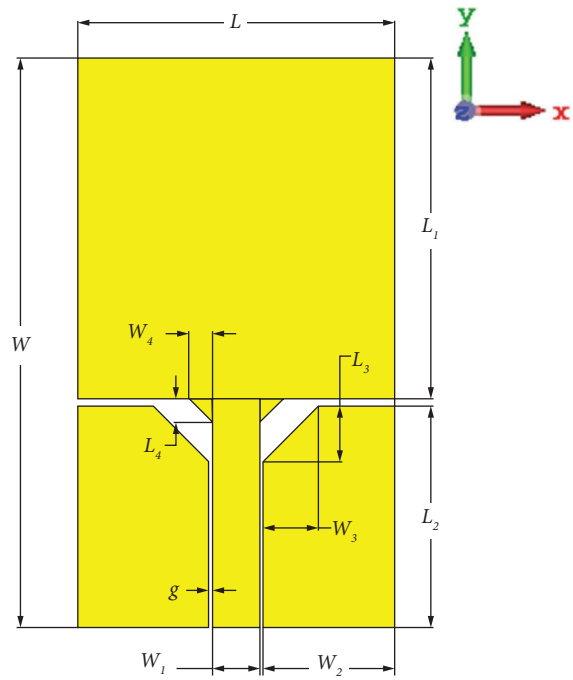

Figure 1: Geometry of the proposed antenna.

Table 1: Structural dimensions of the antenna.

Parameters	Values (mm)
W	50.4
L_1	30.1
L_2	19.6
L_3	4.9
L_4	2.1
g	0.28
L	28
W_1	4.2
W_2	11.62
W_3	4.9
W_4	2.1
H	1

3. FSS Design

Band-stop FSS is often used as a reflector of an antenna because of its excellent reflection characteristics. When the electromagnetic wave is incident on the FSS, the induced current is generated by the electronic oscillation of the metal layer, resulting in a secondary radiation field. At the resonant frequency, the incident radiation field is cancelled out by the secondary radiation field, the electromagnetic wave cannot pass through the FSS, thus the total reflection occurs.

The design evolution of the proposed FSS unit cell is illustrated in Figure 7, and the corresponding parameters are shown in Table 2. The optimal structural parameters are obtained through the parameter scanning method. A

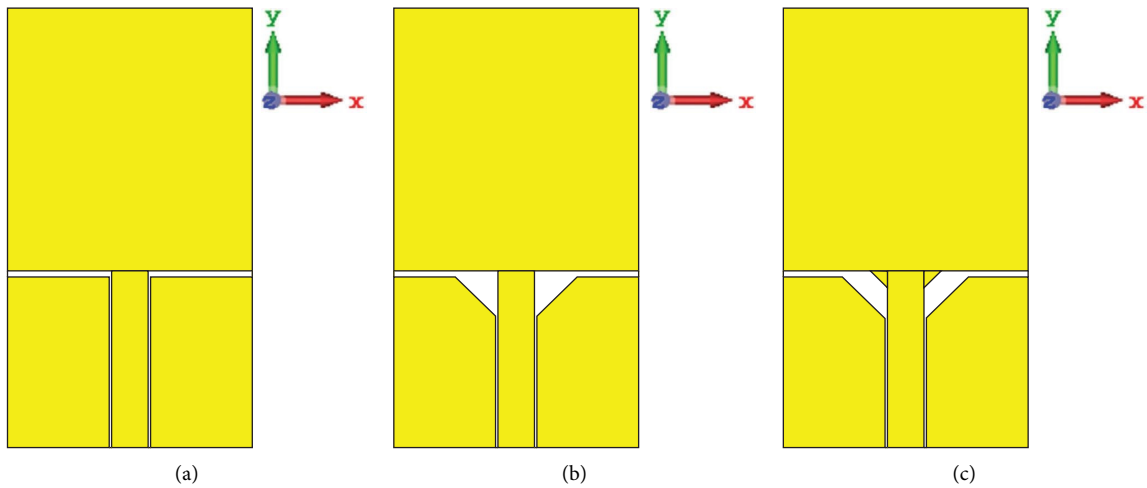

Figure 2: Antenna design evolution. (a) Antenna I. (b) Antenna II. (c) Antenna III.

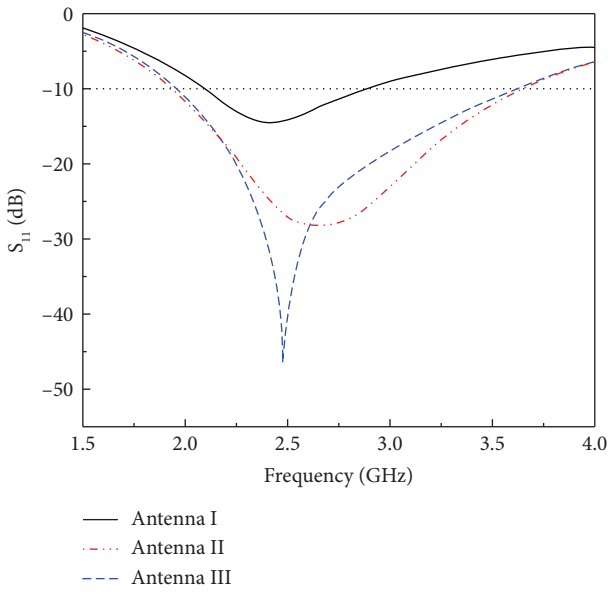

Figure 3: Simulated S_{11} for the different optimized antennas.

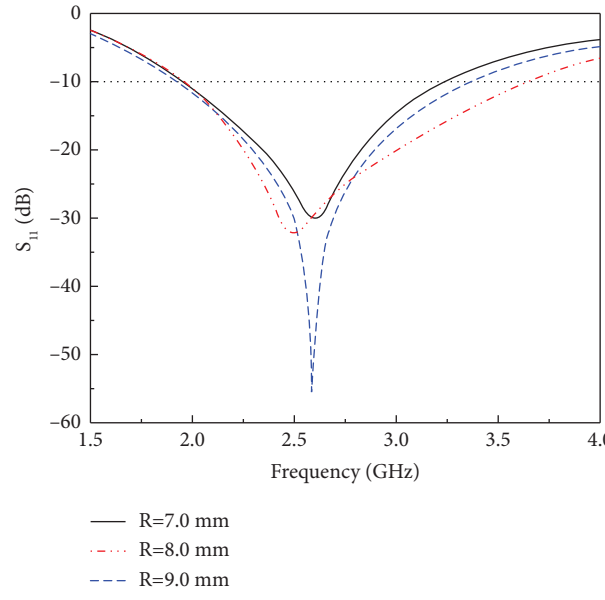

Figure 5: Simulated S_{11} at different bending radii (R).

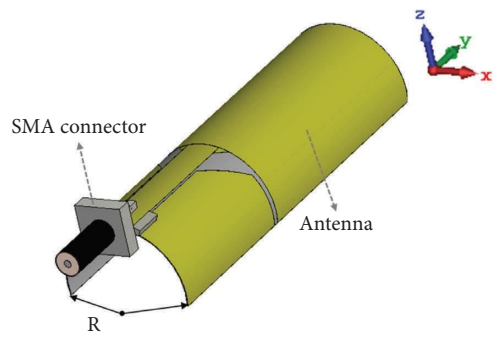

Figure 4: Simulated model of the flexible cylindrical antenna.

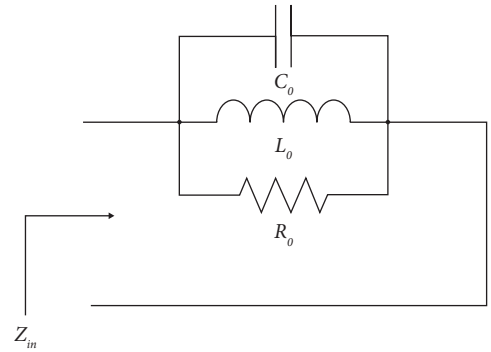

Figure 6: Equivalent circuit model for the proposed antenna.

semiflexible dielectric substrate FR-4 with dielectric constant 4.3, thickness 0.25 mm, and loss tangent 0.0025 is used. Initially, as shown in Figure 6(a), the unit cell starts with a traditional circular structure, which is named Unit cell I. The wavelength corresponding to the resonant frequency is related to the effective length of the ring. For Unit cell I, the

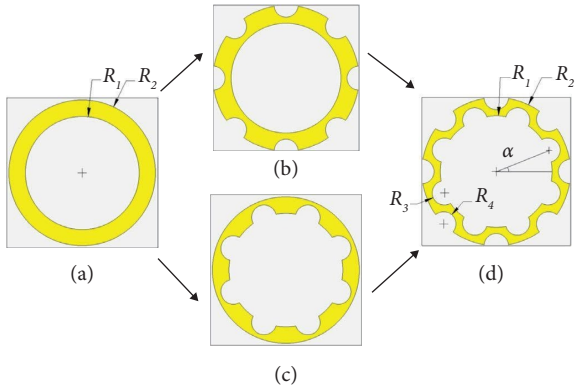

Figure 7: Design evolution of the FSS unit cell. (a) Unit cell I. (b) Unit cell II. (c) Unit cell III. (d) Unit cell IV.

Table 2: Structural dimensions of the FSS unit cells.

Parameters	Values (mm)
R_1	12.8
R_2	17
R_3	2.8
R_4	2.8

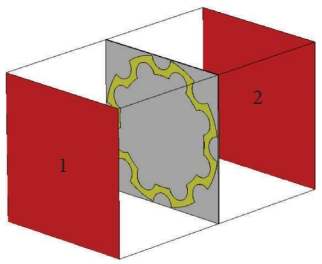

Figure 8: Simulated model of the FSS unit cell.

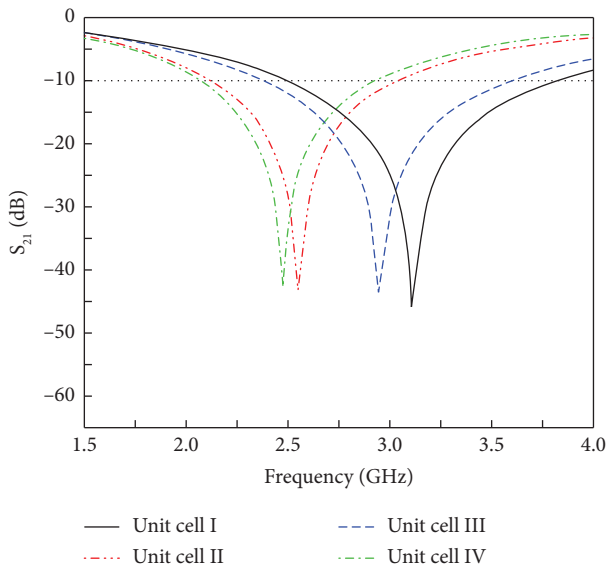

Figure 9: Simulated S_{21} for different unit cells.

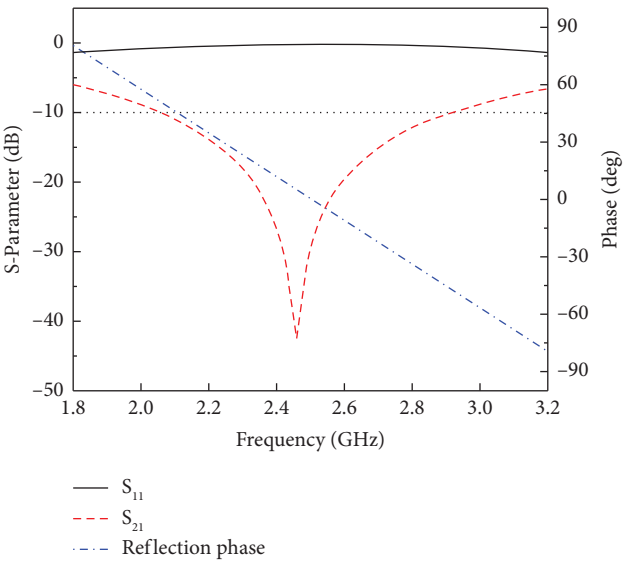

Figure 10: Simulation results of S parameters and reflection phase for the proposed FSS unit cell.

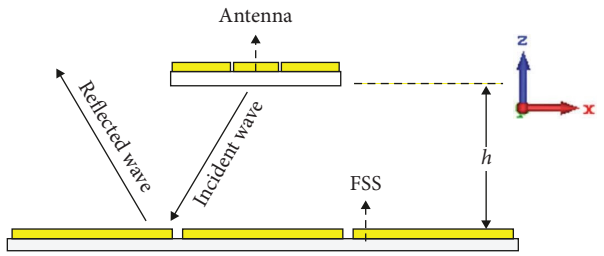

Figure 11: Planar integration schematic.

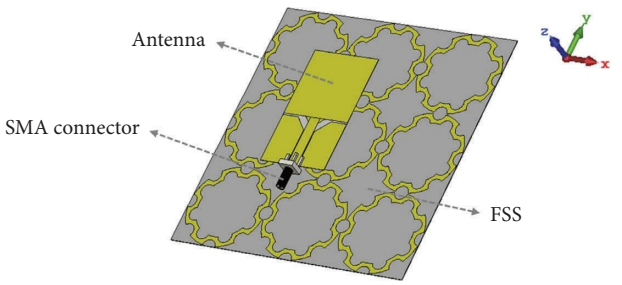

Figure 12: Simulated model of the planar antenna with planar 3 × 3 array FSS.

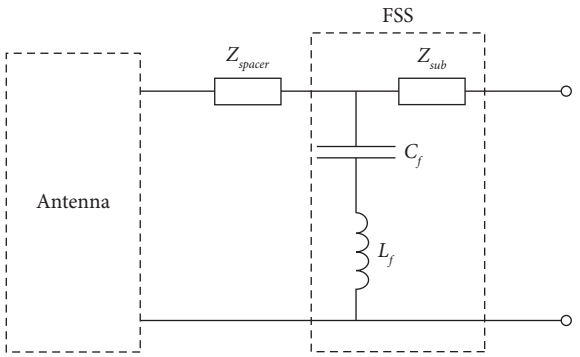

Figure 13: Equivalent circuit model for the FSS with the antenna.

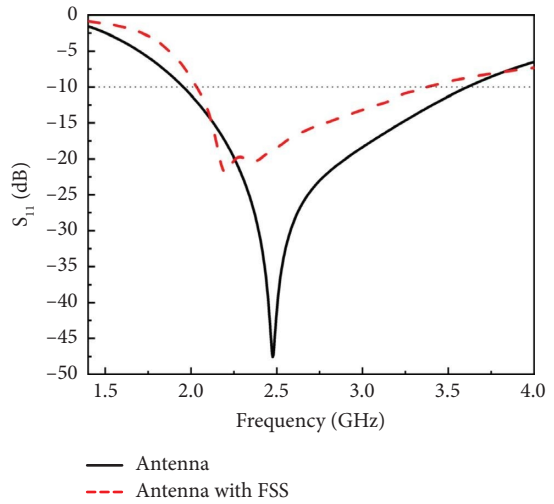

Figure 14: Simulated S_{11} for the antenna with and without FSS.

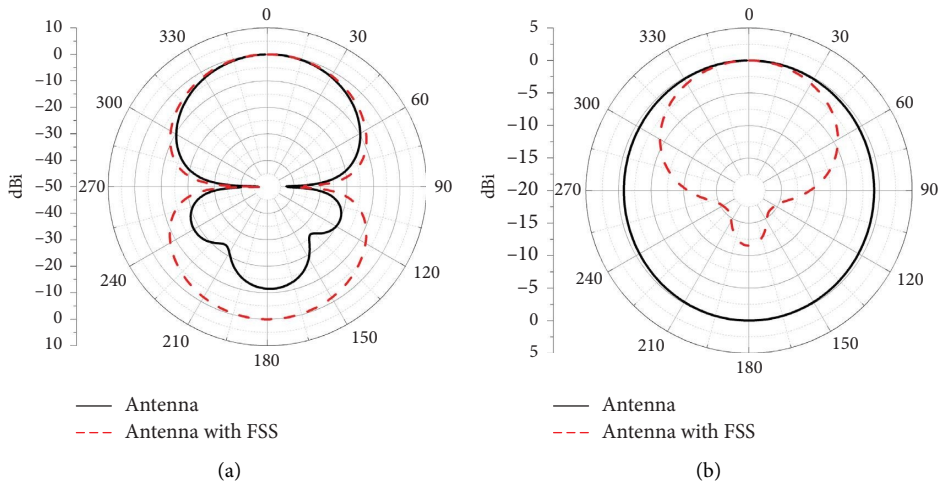

Figure 15: Simulated radiation patterns for the antenna with and without FSS at 2.4 GHz of (a) YZ plane and (b) XZ plane.

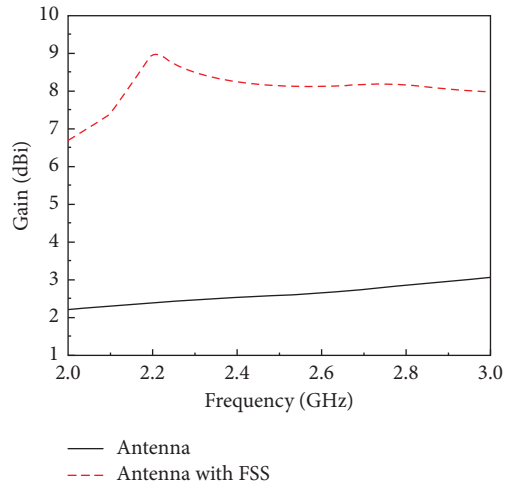

Figure 16: Simulated peak gain for the antenna with and without FSS.

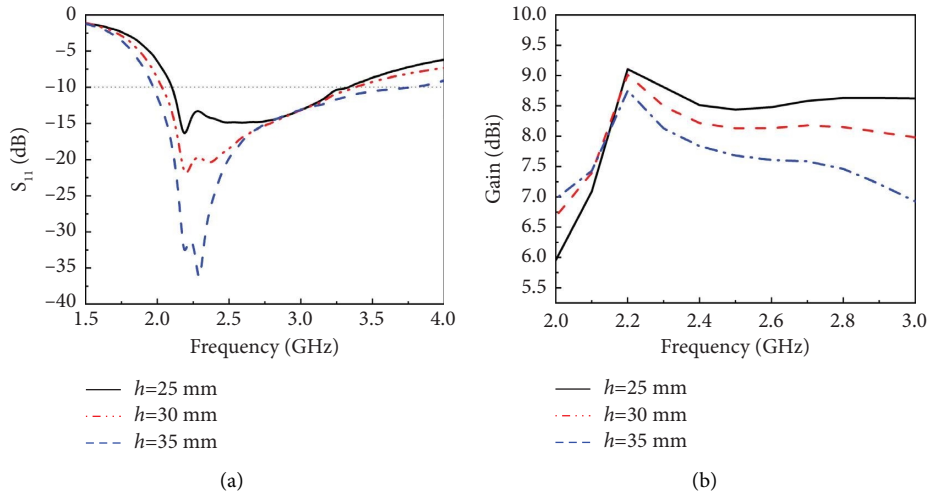

Figure 17: Simulation results for the planar antenna with the planar FSS at different heights (h). (a) S_{11}. (b) Realized gain.

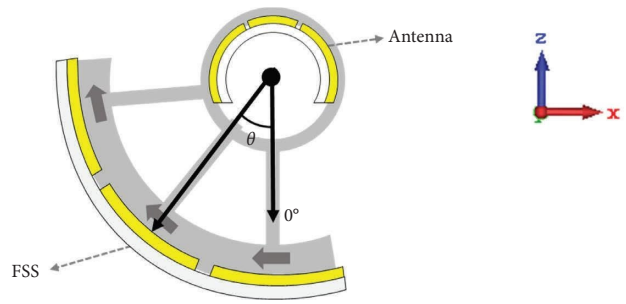

Figure 18: Flexible cylindrical antenna with rotatable curved FSS.

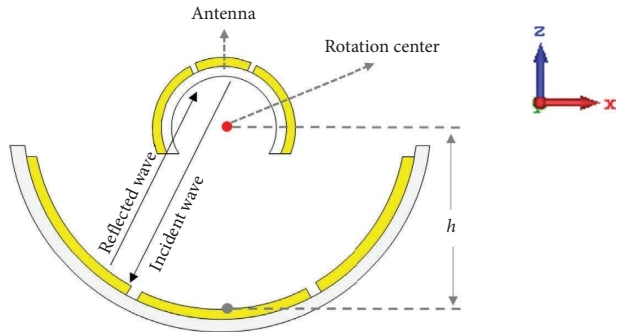

Figure 19: Bending integration schematic.

equivalent length can be regarded as the circumference of the ring [20], and the resonant frequency can be approximated by the following formula:

$$f_r = \frac{c}{2\pi r}, \tag{2}$$

where c is the free space light speed, the effective radius is predicted as $r = (R_1 + R_2)/2$. Based on the parameters in Table 2, f_r is calculated as 3.21 GHz.

The final optimized unit cell (namely Unit cell IV) is depicted in Figure 7(d). The meandering technology is used to achieve miniaturization. The inside and outside of the circular structure are cut off by several semicircles. The effective length of Unit cell IV can be approximated by the arc length of these semicircles. So, a new formula for calculating the resonant frequency is obtained as follows:

$$f_r = \frac{c}{n\pi(R_3 + R_4) - 4n(R_3 + R_4 - 2R_1 \sin(\alpha/2))}, \tag{3}$$

where n is the number of inner or outer semicircles. When α is 22.5° and n is 8, f_r is calculated to be 2.48 GHz. Obviously, the resonant frequency of Unit cell IV is lower than that of Unit cell I.

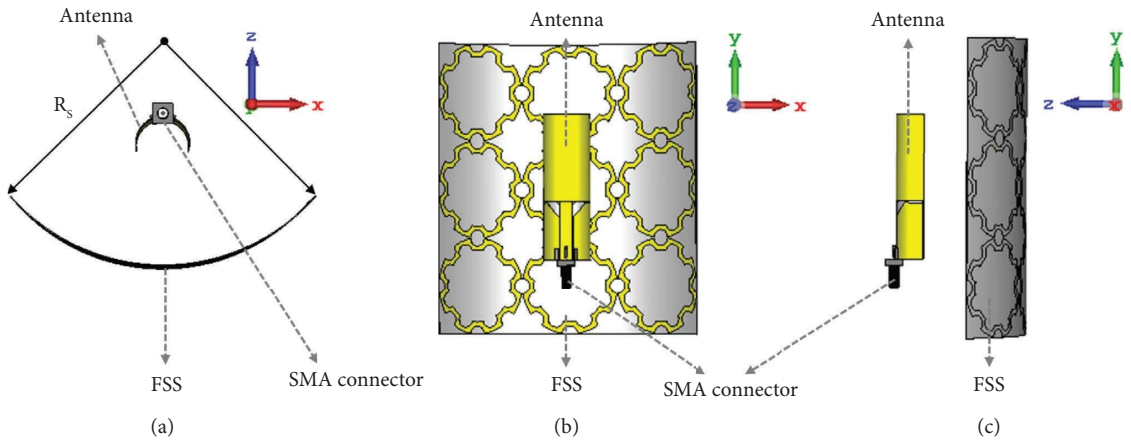

Figure 20: Simulated model of the flexible cylindrical antenna with rotatable curved 3 × 3 array FSS. (a) Front view. (b) Top view. (c) Side view.

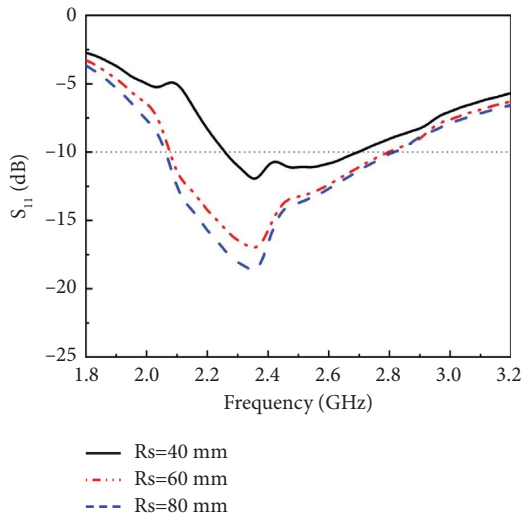

Figure 21: Simulated S_{11} at different bending radius (Rs).

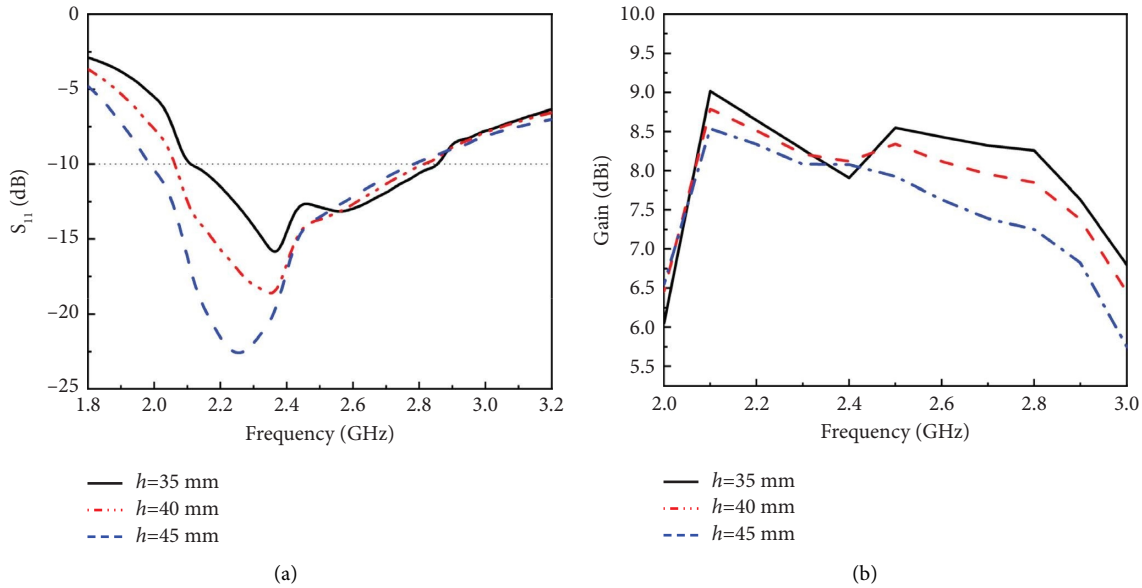

Figure 22: Simulation results for the bending antenna with curved FSS at different heights (h). (a) S_{11}. (b) Realized gain.

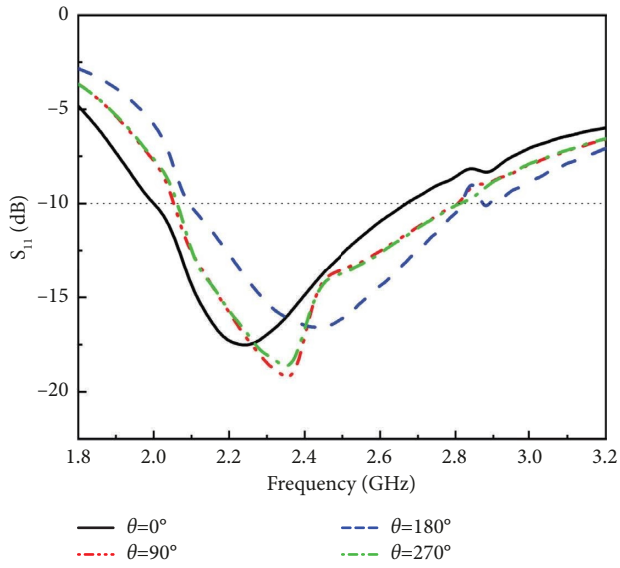

Figure 23: Simulated S_{11} at different rotation angles (θ).

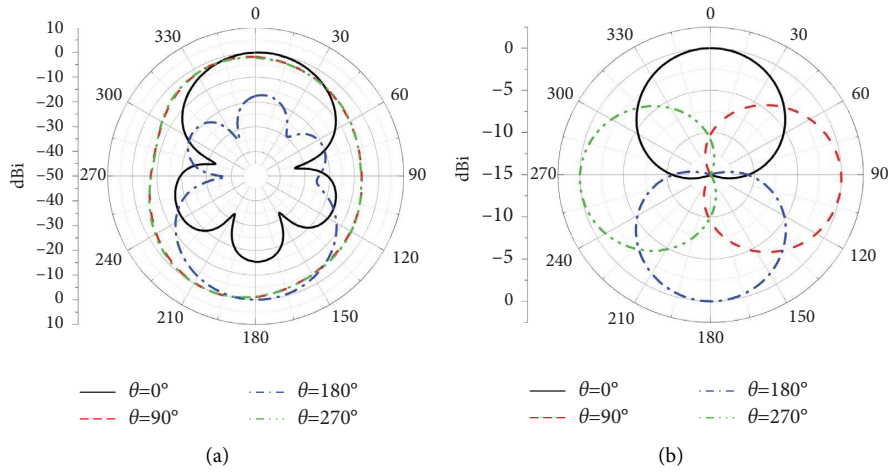

Figure 24: Simulated radiation patterns at different rotation angles (θ) at 2.4 GHz for (a) YZ plane and (b) XZ plane.

The simulated model is shown in Figure 8, and the transmission coefficient (S_{21}) of different structures is shown in Figure 9. Unit cell IV has a lower resonant frequency, which indicates the optimized structure is more miniaturized than the traditional circular structure.

The FSS presents a linearly decreasing reflection phase when it is used as the reflector [21]. The phase of the antenna's radiated wave toward FSS increases with the increase of the frequency. So, the phase of the reflected waves must then decrease with the increase of the frequency to ensure constructive interference at the antenna plane.

The results of the proposed FSS unit cell are shown in Figure 10. The band-stop characteristics are observed in the frequency range of 2.06–2.91 GHz. The reflection phase presents a linearly decreasing trend. The proposed FSS is well matched to compensate the phase of the reflected waves, so as to ensure the realization of the constructive interference.

A reference plane is set with a height of h from FSS. When a uniform plane electromagnetic wave from the reference plane is vertically incident on the FSS, the electric field can be expressed as the following formula:

$$E = \mathrm{A}e^{j\beta z}, \tag{4}$$

where A is the amplitude of the electric field and β is the phase constant.

The phase difference of the electromagnetic wave transmitting from the FSS to the reference plane is $-2\beta h$. φ_{FSS} presents the reflection phase of the FSS. The phase difference of the electromagnetic wave transmitting back and forth between the FSS and the reference plane can be expressed as $\varphi_{\mathrm{FSS}} - 2\beta h$. To ensure constructive interference at the reference plane, formula (5) [21] needs to be satisfied.

$$\varphi_{\mathrm{FSS}} - 2\beta h = 2n\pi, n = \cdots -2, -1, 0, 1, 2 \cdots. \tag{5}$$

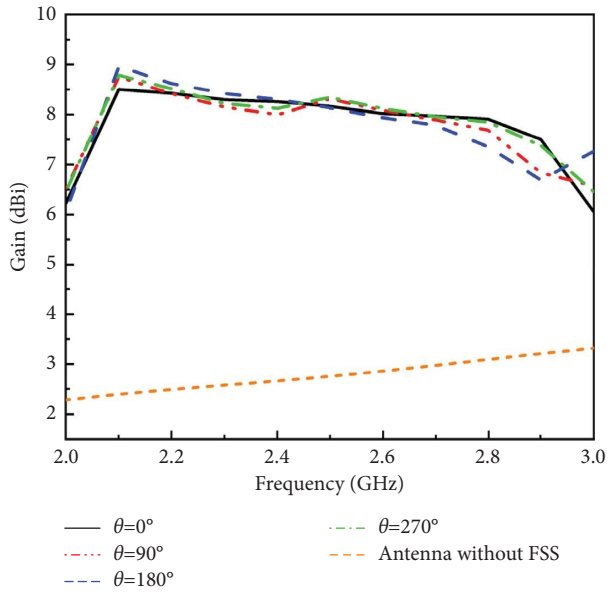

Figure 25: Simulated realized gain at different rotation angles (θ).

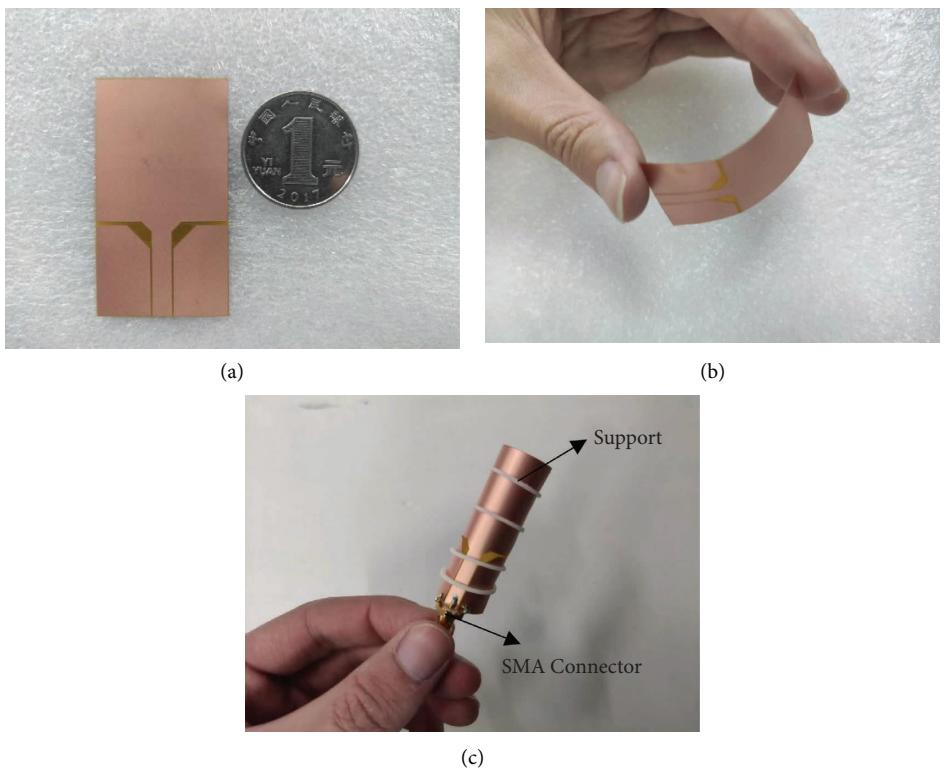

Figure 26: The fabricated prototype of the antenna. (a) Planar view. (b) Bending view. (c) Flexible cylindrical conformal antenna with SMA connector.

λ is the wavelength corresponding to the frequency at which the reflection phase is zero. When h is set equal to $\lambda/2$, then both sides of formula (5) becomes equal.

The proposed planar antenna is applied to integrate with the 3×3 array FSS. The planar integration schematic is shown in Figure 11, and the simulated model is shown in Figure 12. To maximize the effect of the FSS, the antenna is placed at the center of the FSS in the Z-axis direction. After using the FSS, the equivalent circuit model can be considered as Figure 13. The electromagnetic waves from the antenna to the FSS have both oblique and normal incidence. Reference [22] provided the calculation formulas for the lumped

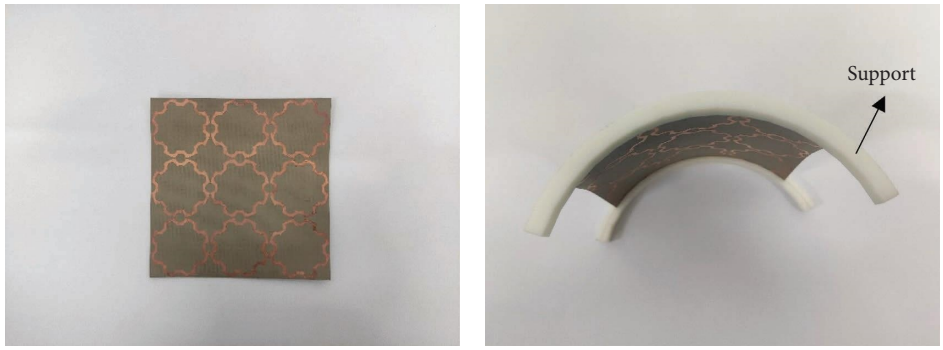

(a) (b)

Figure 27: The fabricated prototype of the FSS. (a) Planar view. (b) Bending view.

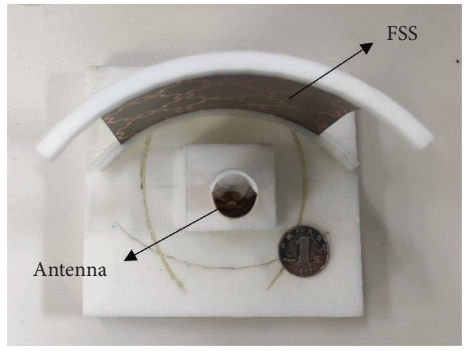

Figure 28: The mechanism in measurement.

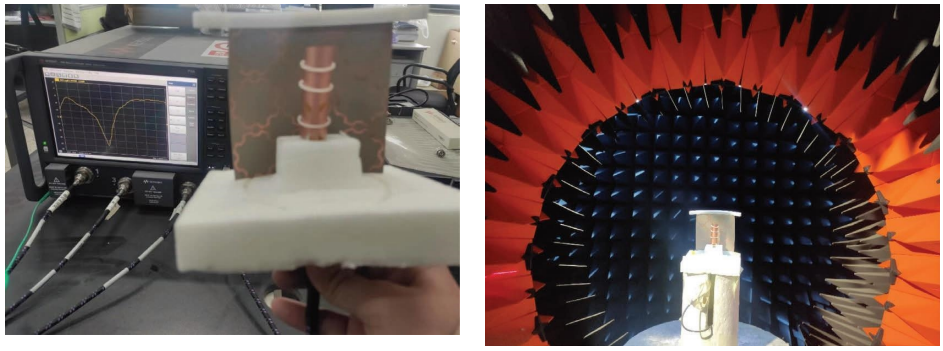

(a) (b)

Figure 29: The measured environment. (a) Vector network analyzer. (b) Microwave anechoic chamber.

parameters in different incidence cases, which indicated these parameters inevitably change in intricate incidence. To achieve the best performance, the optimal distance between the two (h) is determined through simulation, h is initialized to be 30 mm. From the comparison in Figure 14, the impedance matching becomes worse after using the FSS. It is because part of the electromagnetic wave towards the FSS is reflected back to the feed instead of radiating outward. The impedance bandwidth of the antenna with the FSS is 2.03–3.38 GHz, and the percentage bandwidth is 49.91%.

As shown in Figure 15, the radiation characteristics of XZ plane change from omnidirectional to directional, and the radiation in the downside of YZ plane is weakened. As shown in Figure 16, the realized gain increases significantly in the operational band by using the FSS, and the maximum difference is 6.62 dBi at 2.2 GHz.

The simulation results at different h are shown in Figure 17. With the increase of h, the results of antenna gain and the S_{11} parameter seem to be opposite. As the value of the S_{11} parameter is lower, the gain enhancement is weakened. The optimal h needs to be determined by balancing the impedance matching and gain enhancement. By adjusting the value of h, a better S_{11} or higher gain can be obtained.

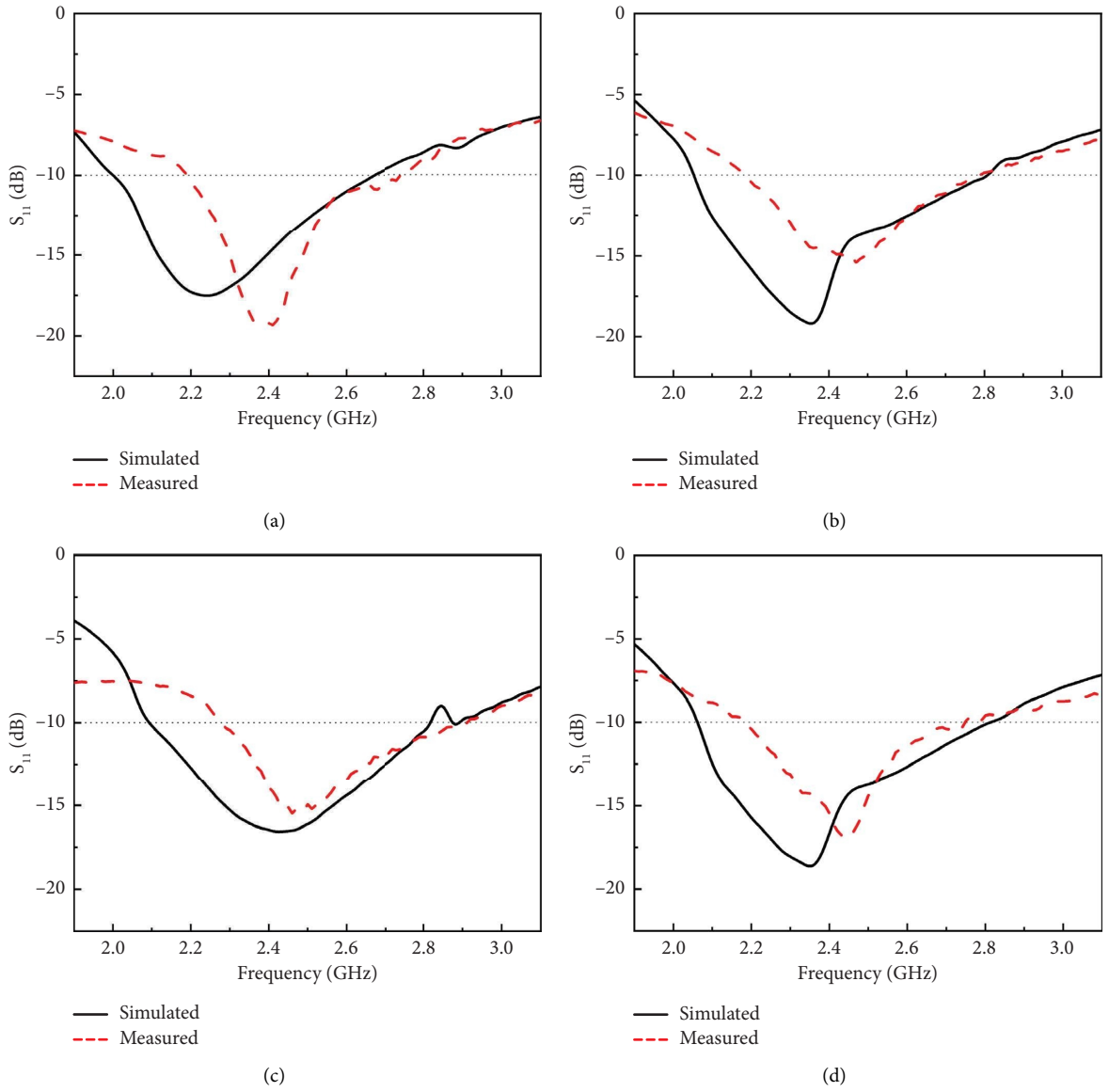

Figure 30: The measured S_{11} of the antenna with FSS at (a) 0°, (b) 90°, (c) 180°, and (d) 270°.

4. Integration of Antenna with Rotatable FSS

The operation of the flexible cylindrical antenna with rotatable curved FSS is shown in Figure 18. The FSS can rotate around the center of the antenna with the rotation angle (θ) of 0–360°.

The bending of antenna and reflector at the same time inevitably affects the performance of the antenna. There are two main reasons as follows: Firstly, a uniform plane wave is applied in the simulation design of the FSS. However, the electromagnetic wave from the antenna cannot be a standard uniform plane wave. Secondly, the characteristics of the FSS show difference between the planar state and bending state. This section described the design law of a flexible cylindrical antenna and rotatable curved FSS through simulation. The bending integration schematic is shown in Figure 19, and the simulated model is shown in Figure 20. The proposed flexible cylindrical antenna with the bending radius $R = 8$ mm is applied to integrate with 3×3 array FSS.

When the distance between the antenna and FSS (h) is set to 40 mm and the rotation angle (θ) is set to 270°, the simulation results of S_{11} at different bending radius (Rs) are shown in Figure 21. In the planar state as shown in Figure 12, partial oblique incidence electromagnetic waves are reflected towards the outside of the antenna. However, in the bending state as shown in Figure 19, these waves return to the antenna and cannot be transmitted outward. With the increase of Rs, the FSS shape is closer to the plane, which is more beneficial for the radiation of the antenna. If the same performance of the antenna is desired to be achieved in the planar state and bending state, h in the bending state should be set larger to compensate for the negative effects of FSS bending.

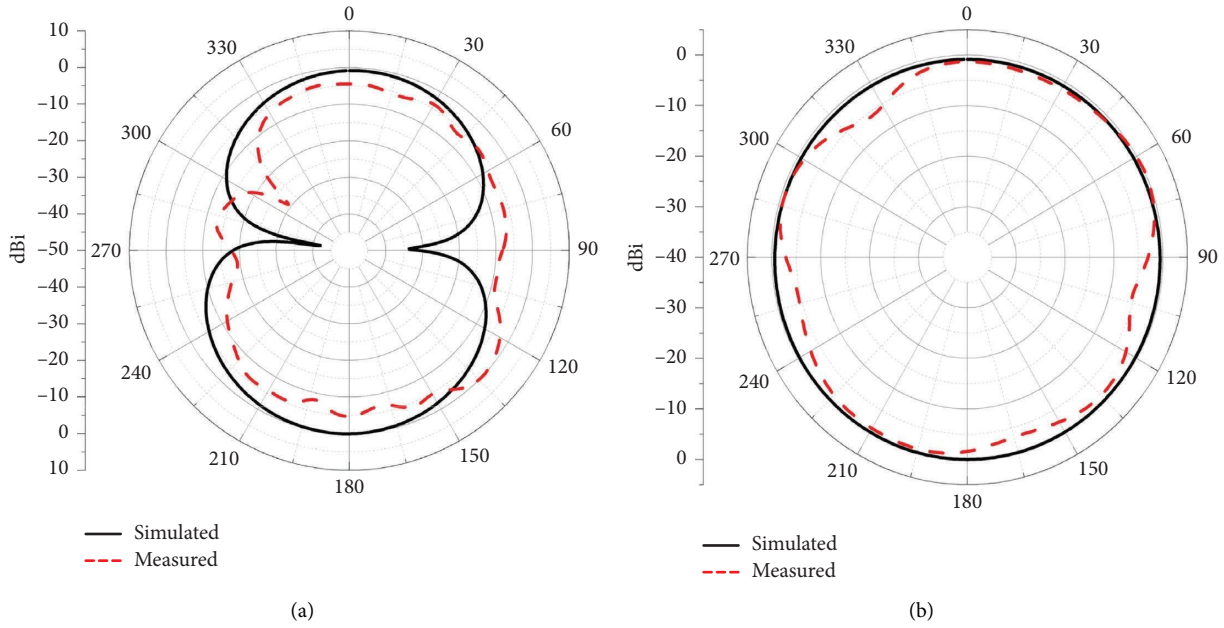

Figure 31: The comparison between the simulated and measured pattern at 2.4 GHz for (a) YZ plane and (b) XZ plane.

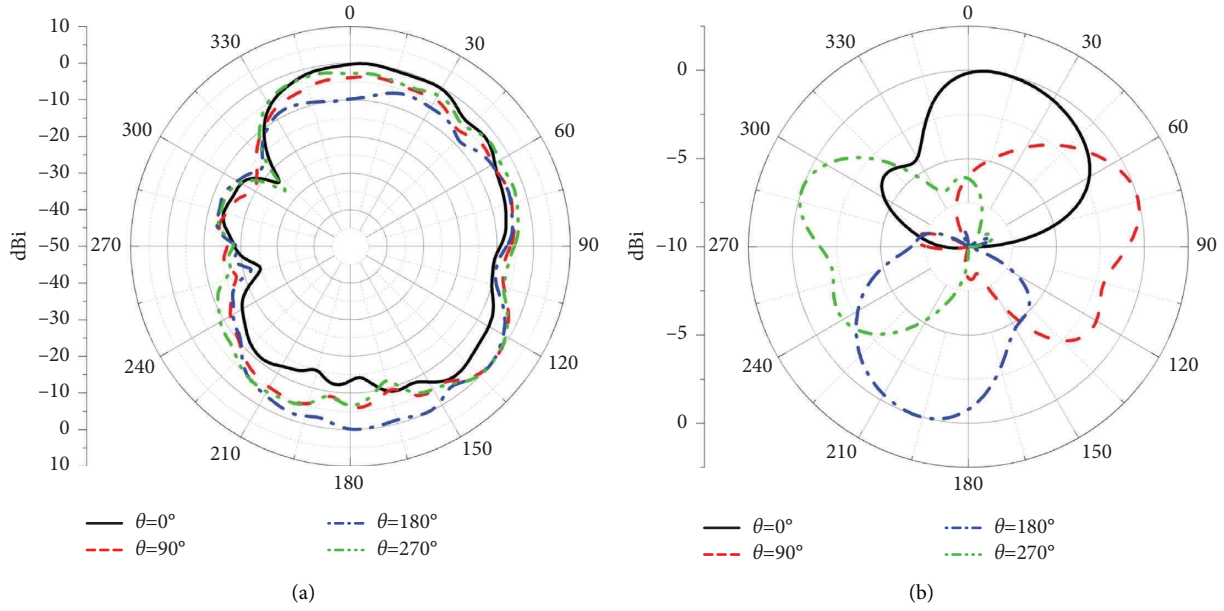

Figure 32: The measured patterns of the antenna with FSS at 2.4 GHz for (a) YZ plane and (b) XZ plane.

The simulation results for the bending antenna with curved FSS at different h are shown in Figure 22. As the value of the S_{11} parameter is lower, the gain enhancement is weakened, which is the same as in the plane state. Similarly, the optimal h needs to be determined by balancing the impedance matching and gain enhancement.

To meet the applications of 2.4 GHz ISM band, h is set to 40 mm and Rs is set to 80 mm. As shown in Figure 18, the curved FSS rotates around the center of the flexible cylindrical antenna, and the rotation angle is denoted by θ. The simulation results of S_{11} at different θs are shown in Figure 23. With the rotation of the FSS, the resonant frequency is slightly shifted. The main reason is that the position of the rotation center is not the feed of the antenna, which results in a different distance between the FSS and the feed. The maximum operational bandwidth is 2.00–2.82 GHz, and the percentage bandwidth is 34.02%.

The radiation patterns are shown in Figure 24. The electromagnetic wave can radiate towards 0–360° with high gain at the XZ plane. For the YZ plane, when the FSS is rotated to the downside ($\theta = 0°$) and upside ($\theta = 180°$) of the antenna, the patterns are obviously weakened on the

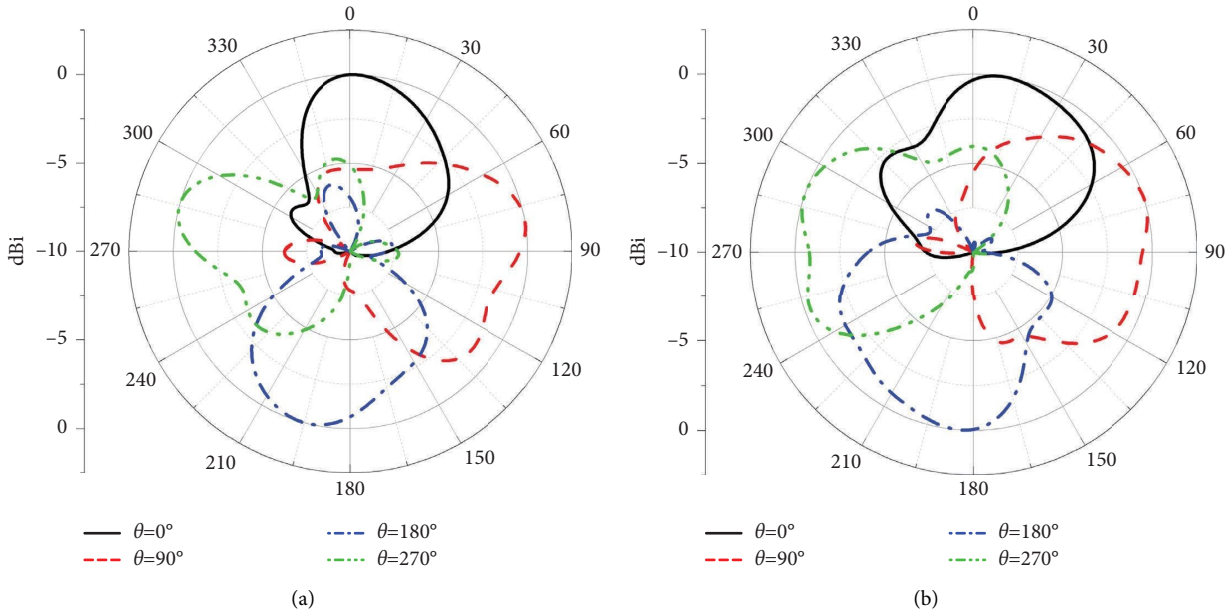

Figure 33: The measured XZ plane patterns at (a) 2.2 GHz and (b) 2.6 GHz.

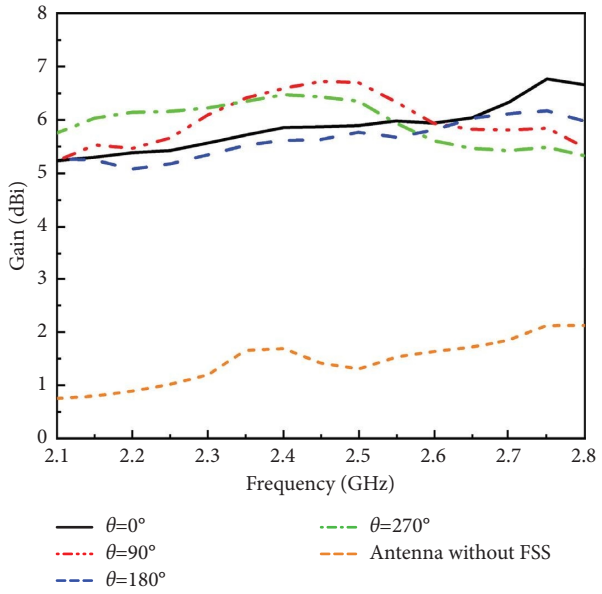

Figure 34: Measured realized gain.

Table 3: The comparison between this work and other relevant works.

References	Feeding method	Flexibility	Operating band (GHz)	Maximum enhanced gain (dBi)	Directivity
[23]	CPW feed	No	2.2–4.8	4	Directional
[24]	Coaxial probe	No	2.4/3.5/5.5	4.4	Directional
[25]	Microstrip feed	No	2.37–2.56/5.15–6.22	3.56	Directional
[26]	Microstrip feed	No	2.38–2.7/3.28–5.8	5	Directional
[27]	Microstrip feed	No	2.4	~5	Directional
[28]	Microstrip feed	No	2.3–2.62/4.9–6.45	4.6	Directional
[29]	CPW feed	Yes	2.4	4.81	Directional
[30]	Microstrip feed	Yes	2.24–2.76	6.3	Directional
This work	CPW feed	Yes	2.18–2.90	5.31	Omnidirectional

opposite side of the FSS, and when the FSS is rotated to the left side ($\theta = 90^{\circ}$) and the right side ($\theta = 270^{\circ}$), the patterns are highly consistent.

The simulation results of peak gain are shown in Figure 25. The realized gain increases significantly in the operational band, and the difference of realized gain with and without the FSS at 2.4 GHz is 5.77 dBi.

5. Measurement and Analysis

To verify performance of the proposed work, the measurement was taken on the fabricated prototype. The fabricated prototype of the antenna and FSS is described in Figures 26–28. As shown in Figure 26(c), the antenna is bent into a cylindrical conformal shape with a radius of 8 mm and is secured by rings made of epoxy. Similarly, the FSS is bent into an arc shape and secured by supports as shown in Figure 27(b). The rotating mechanism between the two is temporarily replaced by foam support, and rotation is achieved by manually changing the FSS rotation angle, as shown in Figure 28.

The measured environment is shown in the Figure 29. The KEYSIGHT PNA Network Analyzer N5224B was used to measure the S_{11} parameter, and the radiation pattern and realized gain were measured in a microwave anechoic chamber.

The comparison between the simulated and measured S_{11} results at different rotation angles is shown in Figure 30. The antenna consistently exhibits a relative bandwidth greater than 20%, covering an operational bandwidth of 2.18–2.90 GHz. There are some discrepancies between the simulated and measured results, mainly manifested in the degradation of the S_{11} parameter at a low frequency. These issues mainly arise from the welding of the antenna and SMA connector. The bending of the antenna increases the difficulty of welding, and the high temperature of the soldering iron causes damage to the PI substrate, resulting in an impact on the feeder of the antenna. Moreover, the supports used in the experiment are made of the resin material, which exhibits a high dielectric constant and has a certain impact on the measured results.

Figure 31 shows that the measured XZ plane radiation pattern of the antenna at 2.4 GHz is omnidirectional. However, after loading the rotatable FSS, as shown in Figure 32, its H plane shows significant directionality. With the change of the rotation angle, the beam can be scanned in the range of 0–360°. As shown in Figure 33, this characteristic is also present at other frequency points within the operational bandwidth. The measured realized gain comparison is shown in Figure 34. The antenna's gain can be increased by up to 5.31 dBi. The damage to the feeder caused by the soldering also affects the measured radiation pattern and gain, resulting in some discrepancies between simulated and measured results, mainly manifested in the splitting of the radiation pattern and weakening of the realized gain.

The above measured results demonstrated the feasibility of this work. The comparison between this work and other relevant work is shown in Table 3. The proposed rotatable curved FSS addresses the issue of the reflector's inability to realize omnidirectional high-gain.

6. Conclusions

In this paper, a flexible cylindrical antenna with a rotatable curved FSS is proposed. The FSS unit cell is optimized based on the traditional circular structure. With the rotatable curved FSS, the antenna can realize omnidirectional high-gain radiation in the operational band. Experimental results demonstrate the feasibility of this work, and the measured antenna gain can be increased by 5.31 dBi at most. The proposed antenna with the FSS can be applied to cylindrical conformal devices operating in the 2.4 GHz ISM band.

Data Availability

The data used to support the findings of this study are included within the article.

Conflicts of Interest

The authors declare that they have no conflicts of interest.

References

[1] H. R. Khaleel, H. M. Al-Rizzo, D. G. Rucker, and S. Mohan, "A compact polyimide-based UWB antenna for flexible electronics," *IEEE Antennas and Wireless Propagation Letters*, vol. 11, pp. 564–567, 2012.

[2] S. M. Saeed, C. A. Balanis, and C. R. Birtcher, "Inkjet-printed flexible reconfigurable antenna for conformal WLAN/WiMAX wireless devices," *IEEE Antennas and Wireless Propagation Letters*, vol. 15, pp. 1979–1982, 2016.

[3] M. El Atrash, M. A. Abdalla, and H. M. Elhennawy, "Gain enhancement of a compact thin flexible reflector-based asymmetric meander line antenna with low SAR," *IET Microwaves, Antennas & Propagation*, vol. 13, no. 6, pp. 827–832, 2019.

[4] R. Zhang, J. W. Liu, Y. Y. Wang, Z. B. Luo, B. Z. Zhang, and J. P. Duan, "Flexible wearable composite antennas for global wireless communication systems," *Sensors*, vol. 21, no. 18, p. 6083, 2021.

[5] P. Kumar, T. Ali, and A. Sharma, "Flexible substrate based printed wearable antennas for wireless body area networks medical applications (review)," *Radioelectronics and Communications Systems*, vol. 64, no. 7, pp. 337–350, 2021.

[6] S. Mat Salleh, M. F. Ain, Z. Ahmad, I. S. Zainal Abidin, and C. M. N. Che Isa, "Development of stretchable and bendable polymer wearable antenna for 5G applications," *Express Polymer Letters*, vol. 16, no. 12, pp. 1267–1279, 2022.

[7] Y. Liu, Z. L. Wang, D. Y. Cang, J. S. Gong, and H. W. Qu, "A polyimide-based flexible monopole antenna," *Journal of Materials Science: Materials in Electronics*, vol. 33, no. 3, pp. 1686–1702, 2022.

[8] A. S. M. Sayem, R. B. V. B. Simorangkir, K. P. Esselle et al., "Flexible and transparent circularly polarized patch antenna for reliable unobtrusive wearable wireless communications," *Sensors*, vol. 22, no. 3, p. 1276, 2022.

[9] Y. J. Gong, S. H. Yang, B. Li, Y. C. Chen, F. L. Tong, and C. Y. Yu, "Multi-band and high gain antenna using AMC ground characterized with four zero-phases of reflection coefficient," *IEEE Access*, vol. 8, pp. 171457–171468, 2020.

[10] M. A. Abdelghany, M. Fathy Abo Sree, A. Desai, and A. A. Ibrahim, "Gain improvement of a dual-band CPW monopole antenna for sub-6 GHz 5G applications using AMC structures," *Electronics*, vol. 11, no. 14, p. 2211, 2022.

[11] D. D. Nguyen and C. Seo, "A wideband high gain trapezoidal monopole antenna backed by frequency selective surface," *Microwave and Optical Technology Letters*, vol. 63, no. 9, pp. 32890–2399, 2021.

[12] A. Kapoor, R. Mishra, and P. Kumar, "A compact high gain printed antenna with frequency selective surface for 5G wideband applications," *Advanced Electromagnetics*, vol. 10, no. 2, pp. 27–38, 2021.

[13] A. M. Retnam, K. Sholampettai Subramanian, and D. Perumal, "Additively manufactured frequency selective surface for gain enhancement of sub-6 GHz monopole antenna," *International Journal of RF and Microwave Computer-Aided Engineering*, vol. 32, no. 11, 2022.

[14] A. B. Devarapalli, T. Moyra, and B. T. P. Madhav, "An FSS based broadband elliptical tree shaped antenna with augmented gain for wireless applications," *IETE Journal of Research*, pp. 1–13, 2022.

[15] J. Li, L. Mao, and T. Zhang, "FSS sandwiched dual-frequency reflectarray for mobile communication applications," *Electronics*, vol. 12, no. 4, p. 897, 2023.

[16] A. Kapoor, R. Mishra, and P. Kumar, "Frequency selective surfaces as spatial filters: fundamentals, analysis and applications," *Alexandria Engineering Journal*, vol. 61, no. 6, pp. 4263–4293, 2022.

[17] Y. B. Chaouche, M. Nedil, I. B. Mabrouk, and O. M. Ramahi, "A wearable circularly polarized antenna backed by AMC reflector for WBAN communications," *IEEE Access*, vol. 10, pp. 12838–12852, 2022.

[18] N. Prasad, P. Pardhasaradhi, B. T. P. Madhav, S. Das, W. A. Awan, and N. Hussain, "Flexible metamaterial-based frequency selective surface with square and circular split ring resonators combinations for X-band applications," *Mathematics*, vol. 11, no. 4, p. 800, 2023.

[19] M. S. Alam and A. Abbosh, "Reconfigurable band-rejection antenna for ultra-wideband applications," *IET Microwaves, Antennas & Propagation*, vol. 12, no. 2, pp. 195–202, 2018.

[20] S. N. Azemi, K. Ghorbani, and W. S. T. Rowe, "3D frequency selective surfaces," *Progress in Electromagnetics Research C*, vol. 29, pp. 191–203, 2012.

[21] F. A. Tahir, T. Arshad, S. Ullah, and J. A. Flint, "A novel FSS for gain enhancement of printed antennas in UWB frequency spectrum," *Microwave and Optical Technology Letters*, vol. 59, no. 10, pp. 2698–2704, 2017.

[22] F. Costa, A. Monorchio, and G. Manara, "Efficient analysis of frequency-selective surfaces by a simple equivalent-circuit model," *IEEE Antennas and Propagation Magazine*, vol. 54, no. 4, pp. 35–48, 2012.

[23] N. Kushwaha and R. Kumar, "Design of a wideband high gain antenna using FSS for circularly polarized applications," *AEU - International Journal of Electronics and Communications*, vol. 70, no. 9, pp. 1156–1163, 2016.

[24] G. Varamini, A. Keshtkar, and M. Naser-Moghadasi, "Compact and miniaturized microstrip antenna based on fractal and metamaterial loads with reconfigurable qualification," *AEU - International Journal of Electronics and Communications*, vol. 83, pp. 213–221, 2018.

[25] E. M. F. Fernandes, M. W. B. da Silva, L. da Silva Briggs et al., "2.4-5.8 GHz dual-band patch antenna with FSS reflector for radiation parameters enhancement," *AEU - International Journal of Electronics and Communications*, vol. 108, pp. 235–241, 2019.

[26] J. Ashish and A. P. Rao, "A dual band AMC backed antenna for WLAN, WiMAX and 5G wireless applications," *Applied Computational Electromagnetics Society*, vol. 36, no. 9, pp. 1209–1214, 2021.

[27] M. A. Belen, "Performance enhancement of a microstrip patch antenna using dual-layer frequency-selective surface for ISM band applications," *Microwave and Optical Technology Letters*, vol. 60, no. 11, pp. 2730–2734, 2018.

[28] C. Shi, J. Zou, J. Gao, and C. Liu, "Gain enhancement of a dual-band antenna with the FSS," *Electronics*, vol. 11, no. 18, p. 2882, 2022.

[29] A. Y. I. Ashyap, Z. Zainal Abidin, S. H. Dahlan et al., "Highly efficient wearable CPW antenna enabled by EBG-FSS structure for medical body area Network applications," *IEEE Access*, vol. 6, pp. 77529–77541, 2018.

[30] B. Sugumaran, R. Balasubramanian, and S. K. Palaniswamy, "Performance evaluation of compact FSS-integrated flexible monopole antenna for body area communication applications," *International Journal of Communication Systems*, vol. 35, no. 6, p. 2022, 2022.